OBSERVED ENHANCEMENT OF REFLECTIVITY AND ELECTRIC FIELD IN LONG-LIVED FLORIDA ANVILS

James E. Dye
National Center for Atmospheric Research, Boulder CO

John C. Willett
Garrett Park MD

Submitted to Monthly Weather Review, Sept. 1, 2006
Revised Jan. 21, 2007

Corresponding Author: James Dye
dye@ucar.edu; Cell phone: 720-530-5012; FAX: 303-497-8171
NCAR; PO Box 3000, Boulder CO 80307-3000
EXPRESS Mail: 3450 Mitchell Lane, FL3; Boulder CO 80307-3000

ABSTRACT

A study of two long-lived Florida anvils showed that reflectivity >20 dBZ increased in area, thickness and sometimes magnitude at mid-level well downstream of the convective cores. In these same regions electric fields maintained strengths >10 kV m^{-1} for many tens of minutes and became quite uniform over tens of kilometers. Millimetric aggregates persisted at 9 to 10 km for extended times and distances. Aggregation of ice particles enhanced by strong electric fields might have contributed to reflectivity growth in the early anvil, but is unlikely to explain observations further out in the anvil. The enhanced reflectivity and existence of small, medium and large ice particles far out into the anvil suggest that an updraft was acting, perhaps in weak convective cells formed by instability generated from the evaporation and melting of falling ice particles. We conclude that charge separation must have occurred in these anvils, perhaps at the melting level but also at higher altitudes, in order to maintain fields >10 kV m^{-1} at 9 to 10 km for extended periods of time over large distances. We speculate that charge separation occurred as a result of ice-ice particle collisions (without supercooled water being present) via either a non-inductive or perhaps even an inductive mechanism, given the observed broad ice particle spectra, the strong pre-existing electric fields and the many tens of minutes available for particle interactions. The observations, particularly in the early anvil, show that the charge structure in these anvils was quite complex.

1. INTRODUCTION

Airborne and coordinated radar measurements were made in thunderstorm anvils near Kennedy Space Center (KSC) in June 2000 and May/June 2001 during the Airborne Field Mill II experiment (ABFM II) which was designed to investigate the relationship between electric fields, microphysics and reflectivity in anvils and other clouds and the decay of electric field in anvils. The airborne measurements were made from the University of North Dakota Citation II Jet aircraft and were coordinated with reflectivity measurements made with the WSR-74C 5 cm radar at Patrick Air Force Base, (which was usually preferred for our analyses because it completed volume scans in 2 1/2 min) and the NEXRAD WSR-88D 10 cm Doppler radar at Melbourne, Florida. Descriptions of the two radars, the airborne field mill system used to measure the electric field, particle measuring instruments, the Cloud-to-Ground Lightning Surveillance System (CGLSS), and Lightning Detection and Ranging (LDAR) system at KSC can be found in Dye et al. (2004) and Dye et al. (2007).

The ABFM II observations in anvils showed that as the aircraft flew from the edge of the anvil into the interior, the transition of electric field from ~1 kV m^{-1} to >10 kV m^{-1} was usually quite abrupt even though the particle concentrations and reflectivity increased smoothly (Dye et al. 2007). The abrupt transition to strong fields usually occurred when the Citation entered regions of reflectivity of 10 to 15 dBZ. Dye et al. (2007) suggested that the abrupt increase in electric field was because the charge advection from the convective core did not occur across the entire breadth of the anvil and also because updrafts, and hence the advection of charge from the cores, were not constant in time. The results from a combined set of measurements from 14 flights into

29 different anvils showed that when the average reflectivity near the aircraft was less than about 5 dBZ, the electric field strength was <3 kV m^{-1}. This was an important operational finding because it showed that a radar-based reflectivity parameter could identify regions in anvils in which it is possible to launch the Space Shuttle or other similar space vehicles without the risk of triggering lightning.

In an effort to quantify the decay of electric field in anvils we tried to compare the estimates of electric field decay obtained from a simple model (Willett and Dye 2003) with the observations of electric field in ABFM II anvils. A more complete description of the model and the comparison with ABFM II observations will be presented elsewhere. Comparison of the model estimates with observations proved difficult in part because examination of the time history of the measurements showed "enhanced" or secondary development of electric field, reflectivity and microphysics in some long-lived ABFM II anvils. It is hard to define what we mean by long-lived, but very approximately, anvils that persist for more than an hour. The enhancements occurred tens of kilometers downwind of the convective cores and over spatial scales of tens of kilometers. In these cases, electric fields >10 kV m^{-1} persisted far downwind of the convective cores for many tens of minutes and in one case for more than two hours.

The purpose of this paper is to document the enhancement of reflectivity and electric field observed in two different anvils and to explore possible causes. Detailed observations from the two anvils are presented in Sections 2 and 3. Readers primarily interested in the interpretation of the measurements may wish to focus their attention on Sections 4 and 5, where possible causes of the enhancements are discussed.

2. 13 JUNE 2000

a. Storm Development, Structure and Environment

The anvil investigated on June 13, 2000 was a result of upper-level outflow and divergence from a series of convective cells that initiated, grew stronger and then decayed. The convective phase of this complex of cells lasted for a period of about 2 1/2 hrs with an isolated anvil that persisted for more than 2 1/2 hrs after the parent convection died out. The first small convective cells were visible on the radar near 1845 UTC (all times are given in UTC) but barely reached 7 km MSL (all altitudes are referenced to mean sea level). By 1900 one small cell attained a reflectivity of 35 to 40 dBZ at 7 km and by 1945 one stronger cell had grown to 40 dBZ at 10 km. The cells grew and remained in the general vicinity of X = -90 to -70 km; Y = -70 to -40 km. (All positions are given relative to the WSR-74C radar at Patrick Air Force Base.) By 2020 there was a small anvil that extended 20 km north of the convective core at 10 km. The reflectivity structure at 11 km near 2100 in Figure 1 suggests divergence of upper level winds with one dominant core with a reflectivity >55 dBZ. The 4 and 7 km Constant Altitude Plan Position Indicator plots (CAPPIs) in Figure 1 show remnants of earlier convection to the north of this storm and new convective cells about 50 km to the west. The first cloud-to-ground (CG) flash detected by CGLSS from this multi-cellular convection occurred at about 1910 and the last CG flash was detected near 2135. The LDAR system detected very few sources on this day and the locations of sources were very inaccurate because not all of the LDAR stations were operating properly in June 2000 until the following day. But LDAR does suggest lightning activity began in this storm near 1905 with the last VHF sources from this storm detected near 2200.

Measurements during ascent to the storm showed the 0 °C level to have been near 4.8 km, which was consistent with the rawindsonde released from Cape Canaveral Air Force Station at 2215. The rawinsonde gave winds of 3 - 7 m s^{-1} from the southeast up to 1.5 km altitude, light winds at 2 - 5 m s^{-1} varying from the northeast through south from 1.5 to 4 km, then southwesterly at 2 -4 m s^{-1} up to 9.5 km. At 10 km, where the balloon ascent was terminated, winds had increased to 5.5 m s^{-1} suggesting the possibility of slightly stronger winds above 10 km. The upper-level divergence at 11 km in Figure 1 is consistent with light winds aloft.

The Citation first penetrated the growing anvil from 2047 to 2052 while climbing from 8.8 to 9.9 km about 30 km from the northern edge of the convective core of 35 to 50 dBZ at 7 km. The scalar magnitude of the vector electric field (which we will refer to as electric field strength) during this penetration was highly variable with peak values of 10 - 20 kV m^{-1}. By 2220, 1 ½ hr later, ten additional penetrations had been made back and forth across the anvil at 10 to 11 km altitude. These penetrations all showed peak electric fields of 10 - 30 kV m^{-1}. Measurements of electric field, particle concentrations and the curtain of reflectivity along the aircraft track from 2112 to 2122 are shown in Figure 2 for the west to east cross anvil penetration of Figure 1. In the eastern part of the anvil, away from the region with precipitation approaching the ground, the electric field strength had values of 10 - 20 kV m^{-1} and the vertical component of the field, E_z, was positive. (A positive vertical field component means that a positive test charge would move upward. However, the coordinate system is attached to the aircraft, so the direction of E_z changes during banks.] Note the small scale variation in the electric field traces. There were abrupt increases/decreases of field strength near 2115 and 2120, but the particle

concentrations did not reflect these abrupt changes. As discussed in Dye et al. (2007), the abrupt increase in field was a common feature of the ABFM II measurements in anvils. They concluded that the most likely cause of the abrupt changes in field were that charge being advected from the convective core was not distributed across the entire breadth of the anvil and was not uniform in time due to the episodic nature of the updrafts in these multi-cellular storms.

b. Evolution of the Anvil

The radar structure of the evolving anvil at 7 km is shown in Figure 3 A, B, C and D at roughly half hour intervals from 2150 to 2325. Figure 3 A was ~15 min after the last CG flash in the storm and shows the remnants of dying convection on the far southwest side of the anvil. This core was ~50 km to the south-southwest of the early convection that produced the anvil. Figure 3B shows that the last active convection capable of feeding this anvil had decayed and the start of a penetration at 2225 at 11 km toward the northeast, 50 min after the last CG flash. A penetration in the opposite direction, which started in the tenuous part of the anvil at 2238, is shown Figure 3C. The plane descended from 11 to 9 km to fly near the top of the layer with reflectivity >20 dBZ (Figure 3G). Penetrations were continued back and forth along the axis of the anvil at 9 km (e.g. Figure 3H) until ~2340 when the plane descended to 8 km as the anvil descended and decayed.

The overall position of the anvil changes little between 2150 and 2324 (Figure 3A through 3D) but the anvil at 7 km broadens noticeably between 2150 and 2220. A red square is drawn at the same location in each plot of Figure 3A - 3D with boundaries at X

= -70 and -50 km and Y = -30 and -10 km. Examination of the location of the red squares and the aircraft track in Figure 3A – 3D shows that the aircraft traversed the same approximate location in the middle of this anvil during each of the penetrations shown in Figure 3A - 3D. The aircraft tracks in 3B, 3C and 3D were along the same radial, which was assigned by air traffic control as was the same turning point at the southern end of the track in these 3 plots. Because the anvil location changed very little between 2150 and 2330, because the winds were light, and because the aircraft repeatedly flew in the same approximate region in the middle of the anvil, the radar and airborne measurements within the red square show the changes in anvil properties with time in this region.

Figure 3E, 3F, 3G and 3H show plots of the vertical structure of reflectivity along the aircraft track and the measured electric field along that track, corresponding to the CAPPIs of 3A, 3B, 3C, and 3D, respectively. Each minute corresponds to approximately 7 km of distance along the flight track. The bold, red lines near the bottom of each reflectivity panel show the periods during which the aircraft was flying within the red squares drawn in Figure 3A through 3D and highlight the portion of the anvil of most interest in the following discussion. The aircraft reversed heading during the 10 min periods shown in Figure 3E, 3G and 3H. Thus 3E, 3G and 3H contain measurements from portions of two separate penetrations. The reflectivity curtains in Figure 3E through 3H all show a region with precipitation falling toward the ground. This region of falling precipitation was on the southwestern side of the anvil and is excluded from the following discussion.

c. Anvil Enhancement

We now focus our attention on the measurements made in the anvil within the region delineated by the red squares in Figures 3A – 3D, and highlighted by the red bold lines in Figures 3E – 3H. Figure 3E shows that the vertical thickness of the anvil within the red square extended from 5 to 13 km (with some pixels at 14 km); in 3F the anvil extended from 4 to 13 km; in 3G the anvil was from 4 to 12 km with a couple of pixels at 13 km; and in 3H it was from 3 to 11 km with a few pixels at 12 km. Thus during the period of these plots the bottom of the anvil descended from ~6 to ~4 km (through the melting level near 4.8 km) while the top descended from ~13 to ~11 km.

However, the thickness of the region with >20 dBZ increased during the early part of this period. In 3E the thickness of the reflectivity >20 dBZ was 6 to 9 km; in 3F it was 4 to 10 km; in 3G 4 to 9 km; and in 3H 5 to 7 km. The top of the 20 dBZ contour increased in altitude slightly between 3E and 3F before descending, while the bottom of this contour fell.

As well as increasing in depth, comparison of the area with reflectivity >20 dBZ between 3A and 3B or 3C shows that the region with >20 dBZ reflectivity also grew in horizontal extent. Additionally, the vertical section in 3G shows a few small areas with a reflectivity of 25 to 30 dBZ in a layer between 5 and 7 km. This is greater than the 20 to 25 dBZ observed during the earlier passes shown in either 3E or 3F which were along the same flight path as 3G. These patchy areas of reflectivity >25 dBZ were 4 – 7 km across and are suggestive of weak cellular convection. The last lightning occurred 70 to 80 min before the penetration shown in Figure 3C and the last sign of reflectivity >35 dBZ at 4 km in the main area of convection disappeared at 2150, 60 min before this penetration. We conclude that there was enhancement of reflectivity and an increase in area with

reflectivity >20 dBZ in the middle region of this anvil. This enhancement appears not to have been fed by low level convection from the core, because the convection on the south and west side of the system had decayed much earlier.

The bottom panels of Figure 3E – 3H show the electric field strength (bold line on the logarithmic scale on the right) and E_z, the vertical component (light line on a linear scale on the left). The cross-anvil penetration (Figure 3E) at 11 km altitude, 2 to 3 km below anvil top, shows field strengths in the anvil from 2152 to 2154 of 15 - 25 kV m^{-1} with a maximum field strength of 28 kV m^{-1} at 2153:30. In the anvil, E_z was negative with values comparable to those of the field strength, but as the aircraft approached the precipitating region the polarity changed to positive near 2154:30. Negative E_z observed at 11 km implies negative charge below the aircraft and/or positive charge above the aircraft. This is consistent with the plane flying below or near a positive screening layer with negative charge below. The often used conceptual model of an anvil has the opposite charge arrangement, i.e. positive charge in the middle of the anvil with negative screening layers near the top and bottom of the anvil. In the precipitating region, positive E_z implies negative charge above the aircraft and/or positive below. We were not permitted by air traffic control to make a spiral descent in this anvil, so it was not possible to determine the vertical charge structure.

Figure 3F shows the measurements at 11 km a half hour later, after the top of the anvil had decreased from ~13 to ~12 km. At 2225, near the falling precipitation, the electric field strength was ~3 kV m^{-1} but dropped to <1 kV m^{-1} at 2227. E_z was negative with values of -2 kV m^{-1} at 2225 and -0.5 kV m^{-1} at 2227, but could be considered essentially zero. Because the anvil top had descended the aircraft was now only 1 to 2 km

below anvil top. Even though the field at the aircraft had decreased compared to Figure 3E, it seems likely that stronger field existed lower in the anvil. As discussed earlier, the evolution of the 20 -25 dBZ reflectivity structure suggests enhancement in the anvil rather than decay. Additionally, the penetration a half hour later (Figure 3G, 2250 to 2300), but at the lower altitude of 9.3 km, showed strong negative E_z. The weak fields during this penetration could be explained by the aircraft flying in or slightly above a positive screening layer.

In Figure 3G the aircraft was flying at 9.3 km, near the top of the 20 dBZ layer. Field strengths of 15 - 40 kV m^{-1} with negative values of E_z of comparable strength were observed until 2256. In the middle of the anvil identified by the red square (2250 – 2251 and 2255 – 2257), the greatest fields were 30 -35 kV m^{-1}. After 2256 the field strength dropped to 1- 2 kV m^{-1} and E_z remained negative. Negative E_z is consistent with negative charge below the aircraft and/or positive charge above, in agreement with our inferences from 3E. The fields in 3G (2250 – 2300) remained strong and even somewhat greater than those 1 ½ hour earlier (2112 -2122, Figure 2) or 1 hr earlier (2150 -2200, Figure 3E). The position of the aircraft relative to the charge certainly makes a difference as to the magnitude of the field that is observed, but clearly the fields inside this anvil remained strong over this 1½ hour period and did not diminish in strength.

Note that the field measurements in Figure 3G vary smoothly with much less small scale variation than the field measurements in Figure 2 or in Figure 3E an hour earlier. This smoothness is suggestive of a horizontally extensive, relatively uniform layered structure of charge. The electric field measurements, like the reflectivity evolution and

structure, show that enhancement occurred in this anvil after convection in the core had ceased.

Figure 3H shows the vertical reflectivity structure and electric field for the period 2320 to 2330. Both electric field and the area and vertical span of higher reflectivity have weakened appreciably by this time. The electric field strength was now only 1 - 1.5 kV m^{-1}. Near 2340 the aircraft descended and made two additional penetrations, both at 8 km altitude, (not shown) between 2346 and 0003 along the axis of the anvil before returning to base. Within the area of the red square the field strengths were 1 - 1.5 kV m^{-1} with a maximum field <2 kV m^{-1} at the southern end of the penetrations outside of the red square. E_z was negative during both of these penetrations. The measurements from these last two penetrations, 1 km lower, as well as those in Figure 3H show weakening field strength and reflectivity, which suggest that the anvil (and electric field and reflectivity) had now dissipated.

3. 4 June 2001

a. Storm Development, Structure and Environment

The very long anvil investigated on June 4, 2001 formed as a result of intense multi-cellular convection. The first cells of this system reached 7 km altitude about 1840 just east of Lake Okeechobee about 150 km south of the WSR-74C radar at Patrick Air Force Base. New and successively stronger cells propagated and grew to the north and later northwest of earlier cells. Radar cloud tops of turrets increased from 12 – 13 km near 1900 to 18 – 19 km by 2030. The storm core was most intense from roughly 1945 to 2020 with >55 dBZ at 10 km near 1945 and again in another cell at about 2015.

Near 1925 a small anvil began to appear at 10 km and spread to the east and north as new cells grew. Near 2000 the very strong convection on the north side of the storm began to form an anvil adjacent to the earlier anvil. As the new cells grew and intensified its anvil outflow grew and spread into the older anvil to the south. During the time of the first and second penetrations of the Citation from 2011 to 2017 and 2018 to 2026, this early phase of anvil growth had a north – south width ~50 km and extended downwind 50 to 60 km. By 2100 the anvil length had increased to more than 150 km as additional cells grew to the northwest. By 2250, when the Citation left the anvil to return to base, the anvil was over 225 km long.

The rawinsonde released from Cape Canaveral at 2100 UTC, about 100 km north of the anvil, showed that winds from near the surface to ~6 km were from the east to southeast at 4 – 8 m s^{-1}. Above 6 km winds were westerly increasing from 2 m s^{-1} at 6 km to 18 m s^{-1} at 14 km. This sounding showed the 0 °C level to be at 4.3 km, while the aircraft measurements showed the 0 °C level at 4.5 km during ascent to the storm and at 4.6 km during descent just north of the anvil at 2249.

The first lightning in this system was detected by LDAR at about 1900 with the first CG flash at 1921. This multi-cell storm continued to produce lightning near the convective cores until after 2300, so lightning was occurring in the core region of the storm throughout the period of the Citation investigations. Occasionally from about 2055 to 2135, the VHF sources from LDAR showed that a few flashes extended 50 to 75 km into the anvil from the storm cores, but the VHF sources were primarily in regions of reflectivity >20 dBZ at 7 km. The CG activity was confined to the vicinity of the cores. Figure 4 shows an example of flash activity extending about 75 km from the convective

cores into the anvil, approximately the farthest that lightning did extend into the anvil. Considerable radial scatter and location error of VHF sources can be seen in the figure because of the 75 – 100 km distance between this storm and the LDAR network. Except for the initial penetration from 2012 to 2018, when the Citation flew near the core with lightning nearby, the aircraft never flew in a region in which the VHF sources were closer than 20 km. The flashes did not extend into the region that we discuss below as "enhanced" anvil. When the Citation flew nearest this region with lightning, field strengths of 20 - 30 kV m^{-1} were observed.

Figure 4 shows the location of the storm core (identified by CG flashes and LDAR activity) and the size and extent of the anvil at 7 km and 10 km. By this time the anvil extended somewhat further north at 10 km compared to 7 km, but the reflectivity at 7 km was greater than at 10 km. The reflectivity >20 dBZ at 10 km had a patchy structure. The small, patchy areas of reflectivity >20 dBZ outside of the core first appeared in the anvil at 9 km at about 2020 and can be seen in Figure 5A and 5B and the vertical section in 5E. The maximum reflectivity remained near 9 km with lesser reflectivity at 7 km than at 9 km until ~2045, when patchy areas of reflectivity >20 dBZ, first appeared on the 7 km CAPPIs. These patchy areas were downwind and separated from the region of higher reflectivity associated with the cores. The area with >20 dBZ reflectivity at 7 km grew with time and remained separated from the cores. By ~2100 the area of >20 dBZ was much larger at 7 km than at 9 km but was patchy at both altitudes.

Because the scan strategy of the WSR-74C radar has gaps between successive elevation sweeps of the antenna, even for low elevation angles, and because of the distance of this anvil from the radar, the sampling of the bottom and the far extent of the

anvil was not continuous in space. Consequently, after gridding the data to Cartesian coordinates, CAPPIs often show discontinuities along arcs perpendicular to the radar beam and the bottom of vertical sections often have a stepped, ragged appearance. The arcs can be seen in the 7 km CAPPI in Figure 4 and raggedness can be seen in the base of the anvil in Figure 5.

b. Evolution of the Anvil

The evolution of the anvil at 9 km is shown in the series of CAPPIs in Figures 5A, 5B and 5D. Figure 5C is at 7 km to illustrate the reflectivity growth at 7 km and that the aircraft was flying directly above this region of growth. Only a few scattered pixels of 20 – 25 dBZ were visible on the 9 km CAPPI. Figure 5E through 5H show the curtain of reflectivity and measured electric field for ten minutes along the aircraft track corresponding to the CAPPIS in Figure 5A - 5D. These time periods were selected to show the evolution of reflectivity and electric field in the eastern portion of the anvil as it was sampled at different times by the Citation.

Figure 5A at 2022 to 2025 shows the early anvil and the decaying core of the two intense cells that produced the northern portion of the anvil. At this time the older, southern part of the anvil was longer than the northern part. The second penetration (Figure 5A) from 2018 to 2026 was from south to north at 9.3 km, 30 to 40 km west of the downwind tip of the growing anvil, and through the greatest reflectivity in the anvil at that time. There was a very small area with 20 -25 dBZ at ~9 km but nothing stronger above or below. Figure 5E shows that the base of the anvil in this location was at 6 km in the south and at 7 km in the north. The electric field strength in the southern portion of

the anvil was strong and variable with a maximum of 55 kV m^{-1} at 2022:30, but was weaker to the north in lesser reflectivity with variable strengths of 3 – 10 kV m^{-1}. The vertical component of the field, E_z, was negative throughout the pass, suggesting positive charge above the aircraft and/or negative below.

About twenty minutes later during the next south to north pass from 2039 to 2046, shown in Figure 5B, the anvil at 9 km had extended 30 km further east. The aircraft, now having ascended from 9.3 to 9.9 km, flew a little east of the highest reflectivity (20 – 25 dBZ) in a peak reflectivity of 15 - 20 dBZ. The electric field strength remained strong and variable with a maximum of 46 kV m^{-1} at 2043. E_z was positive in the southern part of the anvil but changed to negative at 2042 in the northern anvil with no changes in aircraft altitude. This polarity change of E_z was not obviously related to reflectivity structure or to changes of particle concentration.

The base of the anvil in Figure 5F was at 6 - 7 km but had one pixel at 5 km which, compared to 6E, shows some descent of the anvil base. The 4 km CAPPI for this time did not show any evidence of the base of the anvil having yet extending down to 4 km. The first definitive evidence of weak reflectivity at 4 km on the 74C radar appeared at 2100 as a narrow band that gradually spread from west to east. (It appeared somewhat earlier at 2045 on the NEXRAD 88D radar.) The location of this band of weak reflectivity at 2122 to 2125 can be seen in the 4 km CAPPI of Figure 4 with the Citation flying directly above it at 9.9 km. Somewhat before 2100 precipitation had descended below the melting level of ~4.6 km in the same region that the Citation was investigating.

The Citation made a south bound penetration (not shown) at 9.9 km from 2051 to 2059 at distances of 15 – 20 km inside the eastern edge of the anvil. The field strength

was briefly 5 - 10 kV m^{-1} in the middle of the anvil and was associated with a maximum in reflectivity of ~15 dBZ. In the tenuous southeastern and eastern part of the anvil, fields were <1 kV m^{-1} from 2157 to 2107.

Figure 5C shows a westbound penetration along the anvil axis at 9.9 km from weak reflectivity near the eastern edge of the anvil into the region of higher reflectivity. The vertical reflectivity structure and electric field measurements for 2110 to 2120 corresponding to this westerly penetration are shown in Figure 5G. There were areas of reflectivity >20 dBZ 3 to 6 km across that are suggestive of weak convective cells. The electric field measurements show variability on a spatial scale similar to that of reflectivity but a direct relationship is not readily apparent. One minute of time corresponds to approximately 7 km distance. The reflectivity of the bottom of the anvil is ragged, and suggestive of tongues of descending precipitation but we can not be certain because of the vertical gaps in radar coverage mentioned earlier. The figure shows that the anvil base was sloping with a base of 6 - 7 km in the east descending to 3 – 4 km further west. Much of the anvil base was now well below the melting level near 4.6 km. There is a suggestion of a very weak bright band at 4 – 5 km in Figure 5G, but it is not distinct and has a maximum reflectivity of only -5 to 5 dBZ.

The field strength at 2110 was ~1.5 kV m^{-1} but increased to >10 kV m^{-1} as the aircraft flew toward the region with higher reflectivity (Figure 5G) reaching a maximum of 27 kV m^{-1} near 2116. The field showed less small scale variability than seen in Figures 5E or 5F. E_z was negative for the first 5 min (approximately 35 km distance) of this constant altitude pass, then changed to positive at 2115 with no discernible association with particle concentrations, which were smoothly increasing in all size ranges during this

penetration. The reverse track of the aircraft along this same radial from 2120 to 2127 (not shown) revealed a similar pattern to that shown in Figure 5G with field strengths of 10 - 25 kV m^{-1} and with a drop to ~2 kV m^{-1} after 2123 in the more eastern part of the anvil.

Because the area of high reflectivity was moving northward, the east to west penetration shown in Figures 5D and 5H was about 15 km north of the track shown in Figure 5C, but was still along the middle of the area with reflectivity >20 dBZ at both 7 and 9 km. Comparison of Figure 5H with 5G, twenty minutes earlier, shows that the reflectivity >20 dBZ had become much more uniform and now extended from 5 to 10 km in altitude.

Both field strength and vertical electric field in Figure 5H show very little small scale variability. Fields of 20 - 35 kV m^{-1} extended over a distance >70 km. Between 2130:00 and 2131:10, as the aircraft descended rapidly from 9.9 to 9.3 km, both field strength and E_z increased (Figure 5H). E_z had changed polarity from negative to positive at 2129:30, just prior to this descent. This change in polarity and the smooth increase in magnitude of both field strength and E_z as the aircraft descended suggest that the aircraft descended through a layer of negative charge, but we can not rule out sloping charge layers or horizontal changes in charge structure. Even though the electric fields were strong over extensive distances and times, no evidence of either IC or CG lightning was seen in this distant region of the anvil, far from the core which was still producing lightning.

c. Anvil Enhancement

The area with reflectivity of 20 – 25 dBZ at 7 km seen in Figure 4C expanded both north/south and especially east/west between 2040 and 2130 and remained separated from the higher reflectivity associated with the core. Comparison of the vertical sections of reflectivity in Figures 5E, 5G and 5H also shows the vertical growth of the region with reflectivity >20 dBZ. In Figure 5E there were only a few pixels of 20 dBZ at 9 km, in Figure 5G the area with 20 dBZ is broken but extends from mostly 6 to 9 km, but in Figure 5H the vertical section of reflectivity >20 dBZ is quite uniform and extends from 5 to 10 km, and even to 11 km near 2131.

Likewise, the 9 km CAPPIs show a greatly expanded area of reflectivity >20 dBZ. The 9km CAPPIs for 2040 - 2043 (Figure 5B) and 2109 – 2112 (not shown) had only a few small, scattered regions of 20 -25 dBZ reflectivity. But by 2130 - 2133 (Figure 5D) there was an area of 20 -25 dBZ at 9 km extending almost 100 km from west to east. Since greater reflectivity did not exist above 9 km, this increase in area at 9 km could not have been the result of large particles falling from above. The increase must have been from growth of particles near that level. Similarly, because there is a gap in the 20 dBZ contour between the region which became enhanced and the core of the storm, it seems unlikely that transport from the storm core was responsible for the expanded area.

The first penetration of this anvil was immediately adjacent to the convective cores from 2011 to 2017. Field strengths of 50 - 60 kV m^{-1} were observed from 2012 to 2015 during that penetration. Using the electric field decay model described in Willett and Dye (2003) and the particle size distributions measured between 2012 and 2016, we estimated that the maximum time to decay from 50 to near 0 kV m^{-1} would be 60 to 90 min. The simple model is expected to give upper limits to the estimated time for field decay,

because it assumes no turbulence, no mixing, no sedimentation of particles and no change in the particle size distribution during the decay, conditions which are clearly violated. Each of the above processes would decrease the time for electric field decay from that in a quiescent, passive anvil. Since the model predicts a linear decay with time in this high field situation, the estimated time for decay from 50 to 25 kV m^{-1} would be about 30 to 45 min. But Figure 5H shows fields of 30 to 35 kV m^{-1} to be present at 2135 to 2137, 80 min after the first penetration. The observed fields of 30 - 35 kV m^{-1} 80 min later are much, much larger than the upper limits predicted by the model.

This conclusion is further substantiated by a "re-visit" analysis that was done for this case. The vector wind at anvil altitude was estimated from radar data and used to "drift" the aircraft track upwind to compensate for the inferred cloud motion. Intersections of the drifted track can then be identified with "re-visits" of the aircraft to specific cloud parcels. The model of Willett and Dye (2003) was then used to estimate the field strength expected at the time of the "revisit". A paper to be published elsewhere will describe the model and the "revisit" analysis in more detail.

A comparison of electric field strength, particle area, and reflectivity measurements between pairs of visits to several cloud parcels for the June 4th case yielded confusing, "impossible" results. The results often showed increases in observed electric field, particle area, and/or reflectivity between the first and second visits of a pair. From this re-visit analysis, as well as from the lack of expected decay of electric field with time discussed above, we conclude that charge separation (as well as microphysical development) must have been occurring in this anvil.

Not only were the reflectivity and electric fields uniform over a broad region by 2130, but the microphysical measurements showed that the particle concentrations were also quite uniform (Figure 6). Although there were small increases in concentration of the small/intermediate sized particles, and smaller increases in the concentration of the particles >1 mm, between 2131 and 2135 as the aircraft flew to the west, overall the concentrations were surprisingly uniform during this entire 15 min period. Particle concentration measurements 70 min earlier during the cross anvil penetration of 5A from 2019 to 2026 are included in Figure 7. The variability in Figure 7 is in sharp contrast to those in Figure 6. All particles observed in these anvils were ice particles. An examination of measurements from the Rosemount Icing Detector (Schild, 2003) showed no supercooled liquid water to be present in any of the ABFM II anvils at the altitudes that were flown by the Citation.

The maximum particle concentrations in Figure 7 during the 2019 to 2226 penetration (Figure 5A) were observed from 2021 to 2022. Figure 8 shows a comparison between the particle size distribution observed during this period and one observed near 2136, 75 min later. Both of the penetrations were at 9.3 km (-32 °C). Aggregates grow at the expense of the small and intermediate sized ice particles so as time progresses one would expect that there would be a decrease in the small to medium sized particles at a given altitude. However, Figure 8 does not show a decrease, but rather a small increase. Even for the largest sizes, which would have been expected to decrease by sedimentation, the concentrations are greater at 2136 than at 2021.

4. DISCUSSION

Measurements from two different long-lived anvils showed evidence that the horizontal area and vertical extent of reflectivity >20 dBZ increased with time. For the June 13th case the magnitude of the reflectivity also increased. Concurrent with the development of the "enhanced" area/thickness of reflectivity >20 dBZ, the electric field strength remained strong for more than an hour with magnitudes >20 kV m^{-1} and became more uniform with greatly reduced small scale variability. Both the uniform reflectivity structure and uniform electric fields extended over many tens of kilometers. For June 4th, the base of the anvil was initially above the melting level, but descended below the melting zone before the observations showed that reflectivity and electric field had become uniform. The same was true for the June 13th case in the middle of the anvil identified by the red square in Figure 3. Most of the larger anvils investigated in ABFM II including those of June 2, 2001; June 10, 2001; June 15, 2001; and June 24, 2001 showed similar behavior with both electric field and reflectivity >20 dBZ becoming more uniform and horizontally extensive. The uniformity of the electric field and reflectivity in the later stages of these anvils was similar to the measurements we made in several extensive stratiform regions that had precipitation reaching the ground, except that precipitation was not reaching the ground in these anvil cases. In the following we explore some possible mechanisms that might have been acting to enhance electric field and reflectivity.

a. Electric field enhancement

As material in the early anvil is advected away from the core, turbulent mixing would be expected to entrain drier air into the anvil (especially at the edges) as it moves

downstream, leading to the evaporation of particles and a reduction in particle concentration, size and reflectivity. Similarly, during this advection of material the field strength is expected to decay as a result of turbulence and bulk conduction currents within and to the outside of the anvil. Estimates of this field decay using the model of Willett and Dye (2003) suggest that, even in the densest parts of these anvils, the field should decay from 50 to nearly 0 kV m^{-1} in 1 to 1½ hrs. These calculations were based on size distributions actually observed in the dense part of these anvils and probably overestimated the actual decay times in passive, evaporating anvils. But the observations of electric field showed that fields of >10 kV m^{-1} persisted for times well over an hour in some anvils. LDAR did not show lightning extending this far into the anvil, so we can rule out deposition by lightning as a source of charge.

To advect new charge and new material such long distances from the core out into the enhanced regions of the anvil in these cases would have taken an hour or more. In the anvil of June 4th, for example, the observed wind speed of ~15 m/s would have required almost two hours to transport a cloud parcel ~100 km. Thus we feel that we can rule out additional transport of charge from the core to explain the prolongation of strong electric fields.

We conclude that a charge separation mechanism or mechanisms must have been acting to prolong the strong electric fields and to increase the area over which strong fields were occurring. Circumstantially, the enhancement seems to have occurred near the time that the anvil base descended below the melting zone. It seems possible that charge separation occurring near the melting zone might have played a role. Stolzenburg et al. (1994, 2005) and Shepherd et al. (1996) from vertical ascents of balloon borne

instruments through trailing stratiform regions of mesoscale convective systems (MCSs) have shown the existence of positive charge density near the melting level for some MCSs. These papers suggest that charge separation resulting from the melting of ice particles may be responsible for the positive charge they observed, but the mechanism is not understood. See Stolzenburg et al (1994) for a good discussion of possible mechanisms. For the 12 cases they examined, Shepherd et al found that the positive charge near 0 °C did not exist in the absence of a bright band. In the June 4th case Figure 5G shows that there was perhaps a very weak bright band with a reflectivity of -5 to 5 dBZ, but it was not well defined. The June 13th case is more complicated because precipitation was falling on the west side of the anvil but a bright band was not evident. It seems possible to us that charge separation associated with ice particle melting may contribute to the continued electrification of these long lived anvils.

In stratiform regions of some MCSs, [e.g. Chauzy et al., 1985, Stolzenburg et al., 2005] a negative layer of charge has been observed near the melting zone. Observations in ABFM II made during ascents and descents through the melting zone in large scale stratiform regions of decaying convection with precipitation reaching the ground suggested positive charge near the melting zone in some cases and negative charge in others. An inductive mechanism of charge separation acting in conjunction with ice particle melting could explain the difference in polarity near 0 °C for different cases, a conclusion also reached by Stolzenburg et al., 2005. The polarity of the charge separation would be determined by the polarity of the pre-existing field. The ABFM II observations clearly show that electric fields >10 kV m^{-1} were present before the anvil base descended to the melting zone in these two anvil cases and also were present in the stratiform cases.

Even if a charging mechanism was acting at the melting zone it is difficult to see how that alone would be sufficient to explain the observations of continued strong fields at 9 to 10 km. A careful examination by Schild (2003) of measurements from the Rosemount Icing Detector showed no evidence of supercooled water in any of the 2001 ABFM II anvils investigated by the Citation. Most of the penetrations were at altitudes of 8 to 11 km (approximately ~-22 to -45 °C). Perhaps supercooled water might have existed at lower altitudes in the enhanced anvils. Without supercooled liquid water the non-inductive charge separation mechanism of ice particle collisions is much less efficient, but laboratory experiments do show that some charge separation, albeit small, does occur even for ice-ice collisions without supercooled liquid water being present (Jayarante et al. 1983; Caranti et al. 1991), and even at a temperature of -45°C (Buser and AufderMauer 1977). Because of the tens of minutes available and the high concentration and broad size distribution of ice particles ranging from frozen cloud droplets through intermediate sized irregular ice particles to large aggregates it seems possible that charge separation via a non-inductive collision process could have occurred, although at a slower rate than in the convective core.

As far as we are aware no laboratory studies have been reported that investigate collisions between small to moderate sized regular or irregular particles and aggregates or other irregularly shaped, diffusionally grown ice particles. Such studies are needed to evaluate the efficacy of the mechanism in these anvils. Almost all laboratory studies on ice particle collisions in the past two decades have investigated collisions of small ice crystals with graupel or rimed surfaces with or without supercooled liquid water being present. Recent studies by Saunders et al. (2007) appears to have resolved the long

standing difference between the results of Takahashi (1978) and those of the Manchester group (e.g. Jayaratne et al. 1983) on the charge reversal temperature. Saunders et al. conclude that the relative diffusional growth rate of the two ice surfaces is the most important factor influencing the sign of the charge transfer and that therefore the supersaturation in the cloud plays an important role. They suggest that mixing between parcels with different supersaturation could influence the sign of the charge reversal temperature. However, their results apply to clouds in which collisions of graupel or other rimed particles with ice crystals are occurring. In our enhanced anvils the particles appear to have been growing by diffusion alone, without supercooled water and riming. There is little, if any, information in the literature on the magnitude of the charge transfer when two ice particles growing by diffusion collide and separate.

It is hard to rule out an inductive ice-ice collision process in this long-lived anvil regime. Historically, two of the main criticisms of the inductive mechanism as the primary charge separation mechanism in thunderstorms were the long time required for the inductive mechanism to generate fields of sufficient strength to be effective and the short contact time during the collisions between fast falling graupel and small ice crystals (Latham 1981). We observed electric fields >10 kV m^{-1} far from the storm core in the early stage of these anvils, thus strong pre-existing fields necessary for the inductive mechanism to act were present. Additionally, the relative fall speed between ice crystals and aggregates which fall at 1 – 2 m s^{-1} is about a factor five less than between ice crystals and large graupel or small hail that fall at 8 - 10 m s^{-1} or more. Thus in a long-lived anvil longer contact times are also available. Although the rate of charge separation might be slow, many tens of minutes would be available for particle interaction and

charge separation. Breakup of aggregates in a strong field during collisions may also be a factor. It should be noted that weak inductive charging could dissipate energy from the storm and not necessarily enhance it. The complexity of mechanisms potentially acting in the anvil warrants further study with numerical models.

b. Reflectivity and microphysical enhancement

In many ways it is easier to suggest an explanation of why the electric fields are enhanced than it is to understand how the region with 20 – 25 dBZ reflectivity grew in area, upwards in altitude, and for June 13^{th,} in magnitude. With the broad size distribution of particles and fall speeds, aggregation is almost certainly active and probably is being enhanced by the strong electric fields present even in the early anvil. We, as well as other investigators using the superb images obtained from the SPEC Cloud Particle Imager (CPI), have seen chain-like aggregates which are highly suggestive of the influence of electric fields. Connelly et al. (2005) recently reviewed earlier laboratory studies on the enhancement of aggregation by strong electric fields, compared images from the CPI with photographs of linear aggregates in the laboratory and qualitatively concluded that strong fields were probably enhancing aggregation. The early studies, [e.g. Saunders and Wahab, 1975] showed that fields of 50 to 100 kV m^{-1} were needed for self collection of similarly sized ice crystals of 30 to 50 μm in concentrations of 4 - 10 cm^{-3}. Our observations close to the core of storms such as June 4th show fields of 50 – 60 kV m^{-1} but none as large as 100 kV m^{-1}. In broad particle spectra such as observed in these anvils, however, it seems possible that aggregation could be enhanced by fields somewhat weaker than 50 kV m^{-1}, but laboratory studies are not available.

The reflectivity history of the early anvil of June 4th suggests that some increase in reflectivity might have occurred between the first cross anvil penetration and the second, which was 20 - 25 km downstream from the first penetration. For the observed horizontal winds of ~15 - 20 m s^{-1} this transport distance would correspond to 15 -20 min for particle transport. Images from the CPI, the 2D-C, and the HVPS from these penetrations were examined for evidence of possible enhancement in aggregation between the penetrations. Both of the passes showed graupel, some rimed plates, many rimed-irregular particles, and many medium to large aggregates (with and without riming). There were a few linear aggregates or other particles with unusually long protrusions of aggregated smaller particles for which strong fields might have had an influence. Fields were >50 kV m^{-1} during portions of both passes. However, this cursory examination failed to show any notable differences in the frequency of chain aggregates between the two passes or between regions with strong fields and those with weak fields. A quantitative assessment of the influence of strong fields on aggregation requires detailed knowledge of the microphysical conditions, electric field and particle history along the particle path.

Aggregation enhanced by strong electric fields seems unlikely to explain the increase in area and altitude of >20 dBZ reflectivity and the growth of the ice particle spectra further out in the anvil. Figure 8 clearly shows that the concentrations of small, medium and large particles all increased at 9.3 km altitude over a 75 min period. We conclude that a weak updraft must have been acting. An updraft could provide a supply of water vapor for additional diffusional growth and, and if strong enough, might lead to the formation of water droplets and possible riming growth of ice particles at lower altitudes within the

anvil. Unfortunately the pitot tubes on the aircraft malfunctioned, probably due to having ingested lots of ice, so we have no measurements of horizontal or vertical winds. An examination of the CPI images near 2136 showed some particles with sharp, angular edges suggestive of growth by diffusion, but others appeared to be slightly rounded. Evidence of riming was not apparent.

What is the source of this updraft or convection? In a recent paper Knight et al. (2004) described the development of convective cells within anvil precipitation (precipitation from an anvil that reaches the ground). The cells that they described ultimately grew above the top of the anvil and attained reflectivity of 40 to 50 dBZ. They suggested that the new convective cells were probably initiated by an instability created from cooling due to the evaporation and melting of ice particles falling into dry air, perhaps by a mechanism first discussed by Findeisen (1940). They presented soundings of temperature, dew-point temperature, and wet-bulb temperature for the day on which these cells grew to illustrate the conditions under which this kind of instability did occur.

The sounding taken at Cape Canaveral, roughly 100 km from the storm, at 2100 on 4 June 2001 is shown in Figure 9. This sounding has a wet-bulb depression of 3 – 5 °C from 800 to 350 hPa (2.2 to 8.3 km) which is similar to the depressions shown by Knight et al. in their Figure 1. It also shows a layer of instability with respect to the wet-adiabat from 550 to 475 hPa (5.1 to 6.1 km). The sounding released from Cape Canaveral at 1500 had even thicker and drier layers at 600 - 575, 450 - 430, and 380 – 345 hPa (4.4 - 4.8, 6.6 – 7.0, and 8.0 – 8.7 km, respectively) than the 2100 sounding in Figure 9. The Tampa Bay 1200 sounding had a deep layer of dry air extending from 5.2 to 8. 2 km. Each of these soundings had dry layers at anvil altitudes and below. Ice precipitation falling into

these dry layers would have evaporated (and melted if below 0°C), cooled the air, and probably formed downdrafts in the zones with heaviest precipitation. In order to maintain mass balance, the air moving downward in downdrafts would have to be compensated by upward moving air, thus creating the possibility for cellular convection.

We commented earlier that on June 4th the reflectivity >20 dBZ at both 7 and 9 km was patchy, as can be seen in Figure 5C and 5D. The vertical reflectivity structure of the 20 – 25 dBZ regions in Figure 5G for June 4th and the 25 -30 dBZ regions in Figure 3G for June 13th are both somewhat suggestive of weak cellular structure. As with the June 4th case, the June 13th case also had wet-bulb depressions of 3 to 5 °C. Although cells with the strength of those described by Knight et al. did not occur within our anvils, it seems quite possible that cooling of the air by evaporation and melting of the falling particles generated small layers with instability that led to weak convection and weak updrafts. Without radar measurements with better spatial resolution it was not possible to follow the continuity of features seen in Figures 3G and 5G. But if convective cells were acting, how did the uniform nature of the reflectivity and electric field in later stages occur? Is the uniformity simply the result of the complete mixing out by these small convective cells or were weak large-scale updrafts acting? We can not tell. The problem needs further investigation with numerical models and field studies.

5. CONCLUDING REMARKS

We have presented evidence of an enhancement or secondary development of reflectivity and electric field in two long-lived anvils that grew from two quite different Florida multi-cellular thunderstorms. The June 13th storm was south of Orlando, entirely

over land. Upper level divergence of the updraft in combination with weak upper level winds contributed to anvil formation. The convective cells on June 4th also formed over land but stronger upper level winds created an anvil that spread 150 -200 km downwind of the initial convection and out over the ocean and the gulf stream. Yet both of these cases, as well as a couple of other cases that we have not presented, produced a horizontally extensive region in which reflectivity and electric fields became uniform and maintained strength.

We speculate that, particularly for the June 4th case, a weak updraft must have been acting in order to explain the increase in area and altitude of the reflectivity structure and in particular to account for the fact that the concentrations of small, intermediate and large particles at 9.3 km remained very similar, even many tens of minutes later, after transport many tens of kilometers downstream. We also suggest that an inductive charge separation mechanism could have been acting at the melting zone similar to the mechanism responsible for the charge layers observed near 0 °C in trailing stratiform regions of MCSs. However, to account for the strong fields at 8 to 10 km, it seems likely that another mechanism or mechanisms was acting at mid-levels in the anvil. With the broad spectrum of particles observed and the tens of minutes available for particle interactions, charge separation at mid-levels might be occurring via a non-inductive or possibly an inductive, ice-ice collision process, although this seems less likely to us.

The observations of electric field show that the charge structure in the early anvil as well as the distant anvil is more complex than the simple view of a layer of positive charge in the middle with negative screening layers at anvil base and top. While flying at constant altitude, typically 9 to 10 km, we often found changes in polarity of the vertical

field that were not obviously related to changes in reflectivity or particle concentrations in different size ranges. They might be explained by sloping layers of charge as has been inferred from the Lightning Mapping Array observations of New Mexico Tech (Rison et al. 1999). The measurements for June 13th (and sometimes on other days as well) are consistent with a layer of negative charge in the middle of the anvil near the top of the highest reflectivity region, of 20 – 25 dBZ.

Understanding what is happening in these long-lived anvils is a topic for future research with both field programs and modeling. Indeed anvil prolongation and/or enhancement might be fairly common. Anvils often form in air masses in which ice particles fall, evaporate and melt in dry layers below the anvil bases. Knight et al., (2004) found that 80% of the Severe Thunderstorm Electrification Precipitation Study (STEPS) soundings from western Kansas and eastern Colorado were capable of generating instability in this way and we also observed several instances in Florida where it may have occurred, but we have not done a systematic study. A shortcoming of this study for assessing the process or processes which might have led to enhancement and probable prolongation of the lifetime of long-lived anvils is the lack of vertical soundings of both electric field and microphysics and of multiple Doppler radar observations. Spiral descents or ascents coupled with multiple Doppler radar, polarization radar, and lightning mapping array observations would aid greatly. This problem not only is of scientific interest but also may have operational importance for launch operations at KSC and for nowcasting. Although these two enhanced anvils did not produce lightning, the electric fields within them were probably of sufficient strength to trigger lightning for many tens of minutes. Fortunately, in addition to the prolongation of strong electric fields, the

reflectivity in these regions also grew or remained strong, so that the radar-based parameter reported in Dye et al. (2007) successfully identified these regions with strong electric fields.

Acknowledgements

We thank the entire ABFM team for their help in field campaigns, analysis and processing of data and their ideas; Frank Merceret and Frank Madura for encouragement and support; Bill Hall for help in processing and displaying the microphysical measurements and discussions concerning them; Carl Schmitt for help in processing and viewing the CPI images; and Charles Knight for helpful comments. This work was supported by NASA contracts CC-90233B, PR 4200097669 and NASA Grant NAG 10-284. The National Center for Atmospheric Research is partially supported by the National Science Foundation.

REFERENCES

Buser, O. and A.N. AufderMauer, 1977. Electrification by collision of ice particles on ice or metal targets, in *Electrical processes in atmospheres*, Editors H. Dolezalek and R. Reiter, Steinkopf, Darmstadt Germany, 294-301.

Caranti, G.M., E.E. Avila, and M.E. Re, 1991. Charge transfer during individual collisions in ice growing from vapor deposition, *J. Geophys. Res.*, **96,** 15365-15375.

Chauzy, S.P., M. Chong, A. Delannoy, and S. Despiau, 1985: The June 22 tropical squall line observed during COPT 81 experiment: Electrical signature associated with dynamical structure and precipitation. *J. Geophys. Res.*, **90**, 6091-6098.

Connolly, P.J., C.P.R. Saunders, M.W. Gallagher, K.N. Bower, M.J. Flynn, T.W. Choularton, J. Whiteway and P.R. Lawson, 2005: Aircraft observations of the influence of electric fields on the aggregation of ice crystals. Quart. J. Roy. Meteor. Soc., **131,** 1695-1713.

Dye, J.E., S. Lewis, M.G. Bateman, D.M. Mach, F.J. Merceret, J.G. Ward and C.A. Grainger, 2004: Final Report on the Airborne Field Mill Project (ABFM) 2000-2001 Field Campaign. NASA/TM-2004-211534, National Aeronautics and Space Administration, Kennedy Space Center, FL, 132 pp. Available from NASA Center for AeroSpace Information (CASI), 7121 Standard Drive, Hanover, MD 21076-1320.

Dye, J.E. et al, 2007: Electric fields, cloud microphysics, and reflectivity in anvils of Florida thunderstorms. Accepted in *J. Geophys. Res.*, Nov. 2006.

Findeisen, W.,1940: Die Entstehung der 0° Isothermie und die Fraktocumulus-Bildung unter Nimbostatus (The origin of 0°C isothermal layers and of fractocumulus beneath nimbostratus). *Meteor. Z.*, **57**, 49-54.

Jayaratne, E.R., C.P.R. Saunders, and J. Hallett, 1983: Laboratory studies of the charging of soft-hail during ice crystal interactions. *Quart. J. R. Meteor. Soc.*, **109**, 609-630.

Knight, C.A., L.J. Miller and W.D. Hall, 2004: Deep Convection and "first echoes" within anvil precipitation. *Mon. Wea. Rev.*, **132**, 1877 – 1890.

Latham, J., 1981: The electrification of thunderstorms. *Quart. J. Roy. Meteor. Soc.*, **107**, 277-298.

Rison, W., R. J. Thomas, P. R. Krehbiel, T. Hamlin, and J. Harlin, 1999: A GPS-based three-dimensional lightning mapping system: Initial observations in central New Mexico. *Geophys. Res. Lett.*, **26**, 3573–3576.

Saunders, C.P.R., and N.M.A. Wahab, 1975: The influence of electric fields on the aggregation of ice crystals. *J. Meteor. Soc. Jpn*, **53**, 121 -126.

Saunders, C.P.R., H. Bax-Norman, C. Emersic, E.E. Avila, and N.E. Castellano, 2007: Laboratory studies of the effect of cloud conditions on graupel/crystal charge transfer in thunderstorm electrification. *Q. J. Roy. Meteor.* Soc., in press.

Schild, J.J., 2003: Liquid water in thunderstorm anvils over Kennedy Space Center, Florida during the summer 2001 ABFM field campaign. M.S. Thesis, Univ. of North Dakota, 55pp.

Shepherd, T. R., W.D. Rust, and T.C. Marshall, 1996: Electric fields and charges near 0°C in stratiform clouds. *Mon. Weath. Rev.*, **124**, 919-938.

Stolzenburg, M., T.C. Marshall, W.D. Rust, and B.F. Smull, 1994: Horizontal distribution of electrical and meteorological conditions across the stratiform region of a mesoscale convective system. *Mon. Weath. Rev.*, **122**, 1777-1797.

Stolzenburg, M., T.C. Marshall, W.D. Rust, E.A. Mareev, and S.S. Davydenko, 2005: Electrical structures in the stratiform precipitation region of mesoscale convective systems, *EOS Trans. Amer. Geophys. Un.*, Dec. 7, 2005.

Takahashi, T., 1978: Riming electrification as a charge generation mechanism in thunderstorms. *J. Atmos. Sci.*, **35**, 1536-1548.

Willett, J. C. and J. E. Dye, 2003. A simple model to estimate electrical decay times in anvils, *Proc. 12th Intern. Conf. on Atmosph. Electr.*, Versailles, France, June 2003, 267-271.

"Pages missing from available version"

Figures for Anvil Enhancement manuscript
by Dye and Willett

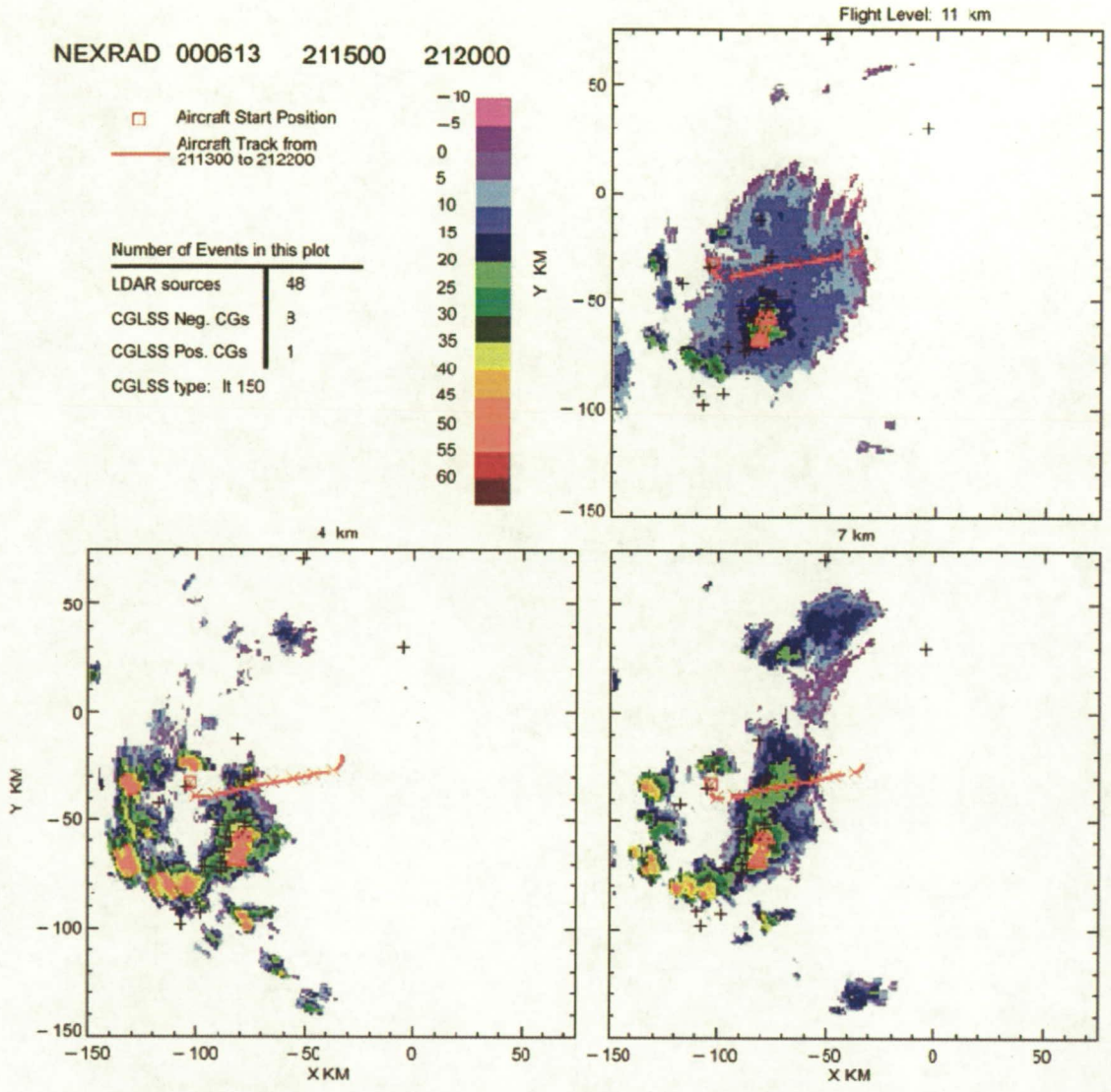

Fig. 1. CAPPIs at 4, 7 and 11 km MSL for the 2115 – 2120 NEXRAD volume scan on 13 June 2000. The Citation track from 2113 to 2122 is overlaid in red with the initial position shown by a square and Xs showing each successive minute along the track. Red triangles show the positions of CG flashes detected by CGLSS during this volume scan. The ground projection of LDAR VHF sources are shown by black pluses.

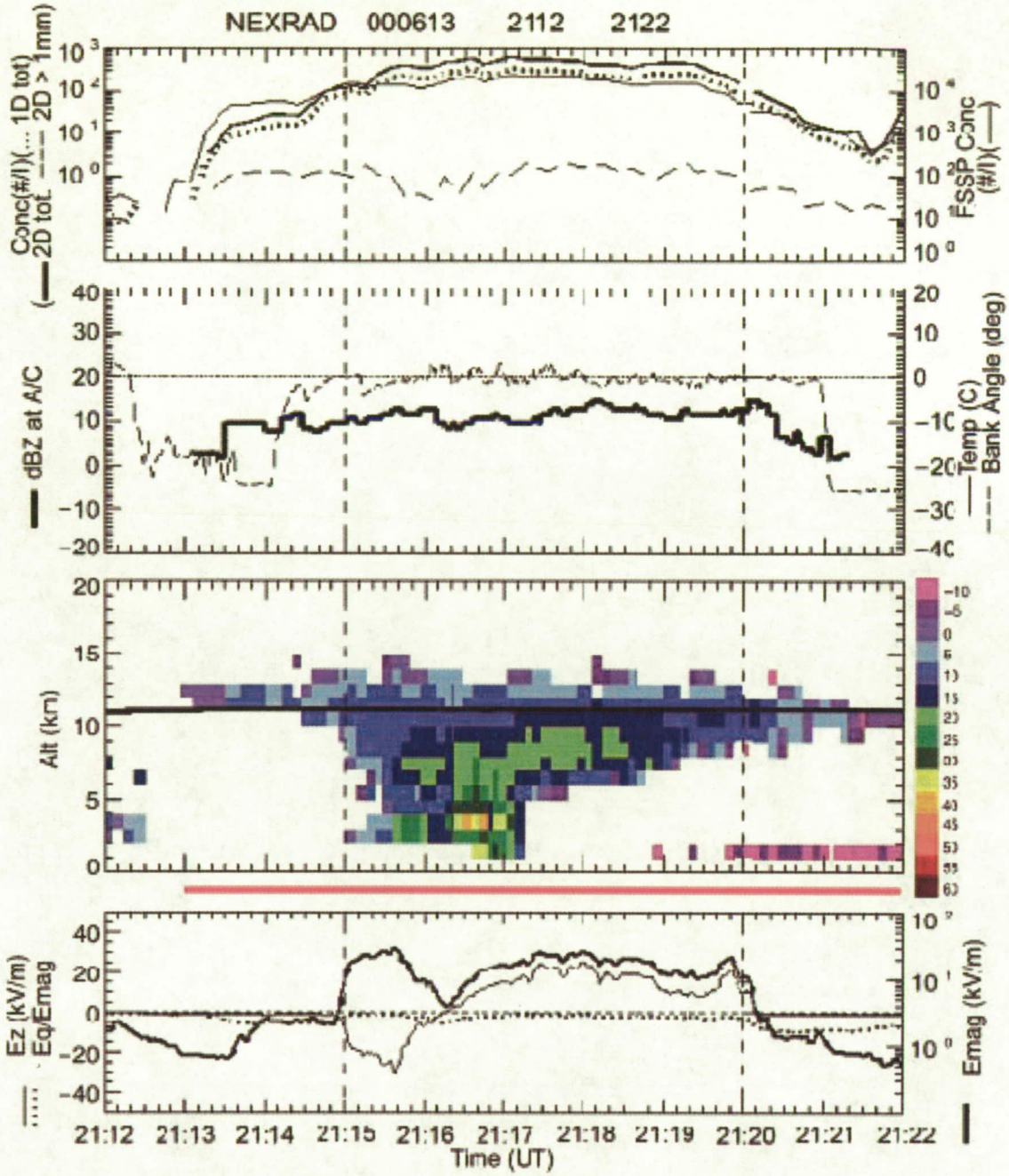

Fig. 2. Airborne and radar measurements on June 13, 2000 from 2112 to 2122: Top Panel: Particle concentrations from different instruments: FSSP total concentration = light, solid line; 2D-C total concentration = bold, solid line; 2D-C concentration >1 mm = dashed line; 1D-C total concentration = dotted line. Second panel: Reflectivity at the aircraft location, and bank angle of the aircraft. The ambient temperature was -46 °C and is off scale in the plot. Third Panel: Curtain of radar reflectivity above and below the aircraft (the numbers to the right show the upper limit of reflectivity for each color interval); bold line = aircraft altitude. Bottom panel: Ez, the vertical component of electric field, is a thin line and referenced to the linear scale on the left. Eq/Emag is a dotted line, also on the left scale. (Eq is the field due to charge on the aircraft). Emag, the

scalar magnitude of the vector field, is a bold line and referenced to the log scale on the right. The vertical dashed lines show the boundaries between different radar volume scans. The red bar below the third panel corresponds to the time of the aircraft track shown in Figure 1.

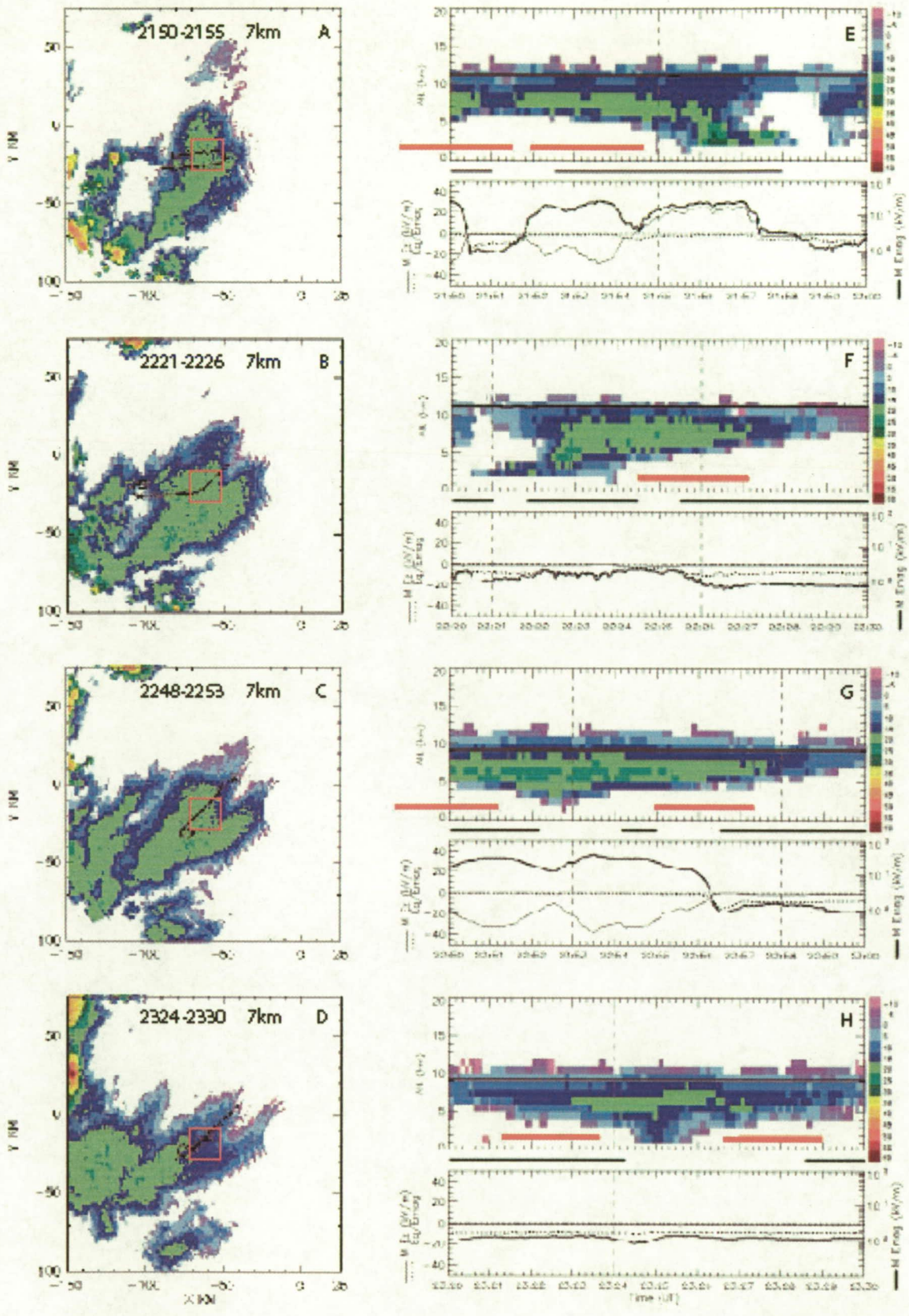
2150-2155 7km A
2221-2226 7km B
2248-2253 7km C
2324-2330 7km D
E
F
G
H
Y (km)
X (km)
Time (UT)

Fig. 3. A, B, C and D are CAPPIs from the Melbourne FL NEXRAD radar showing the evolution of the anvil at 7 km on 13 June 2000. Nine minutes of aircraft track are in black superimposed on each CAPPI centered on the time of each radar volume scan. The red square identifies the same region in each plot. See text. E, F, G and H are similar to Figure 2 but show only the curtain of reflectivity and electric field measurements for 10 min of aircraft measurements corresponding to the CAPPIs of A, B, C and D, respectively. The bold, red lines show the periods when the aircraft was flying within the red square in A, B, C and D. The black lines between the top and bottom panels show when the aircraft was flying straight and level.

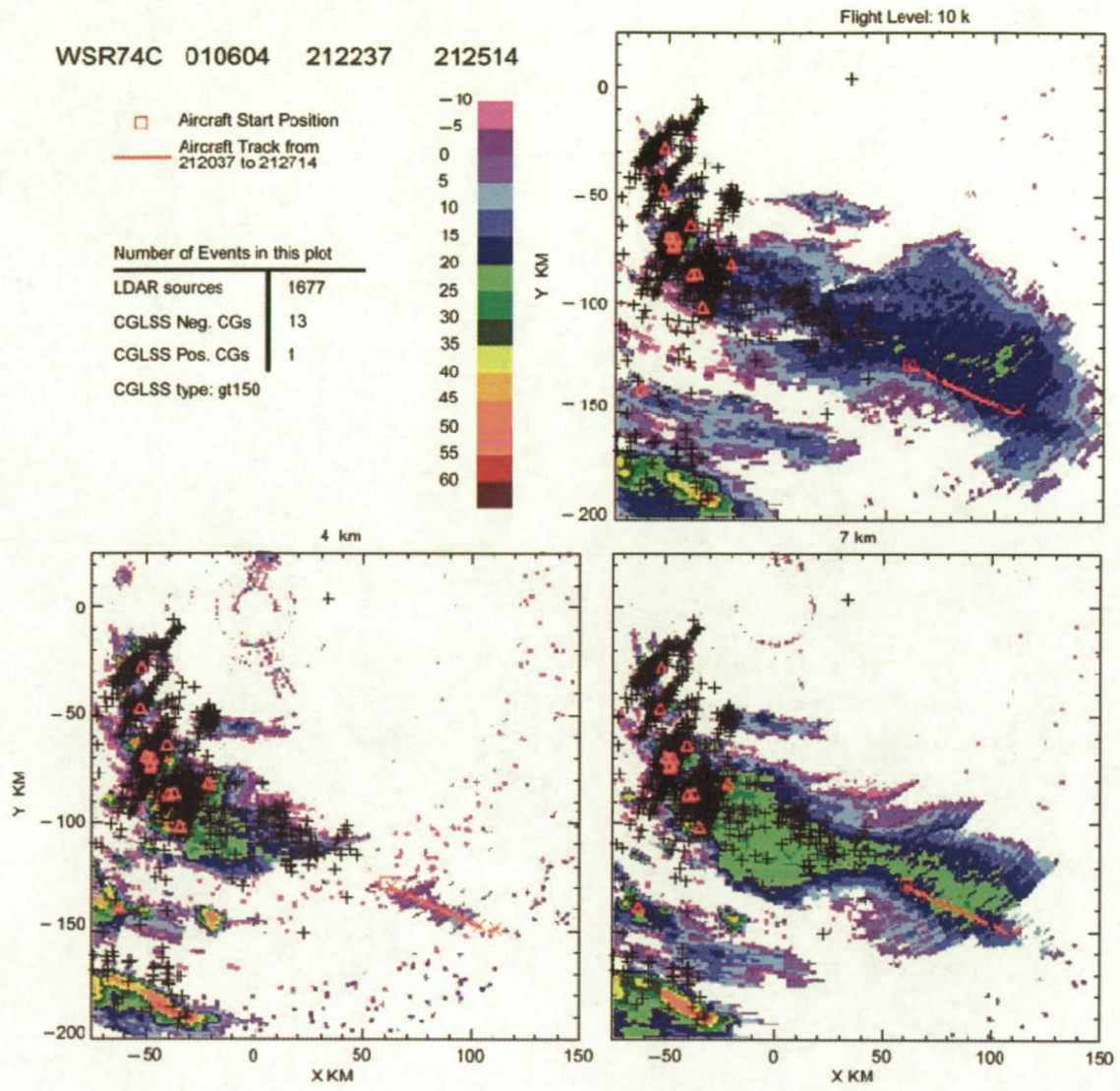

Fig. 4. Same as Fig. 1 for the 2122:37 – 2125:15 volume scan of the WSR-74C radar on 4 June 2001.

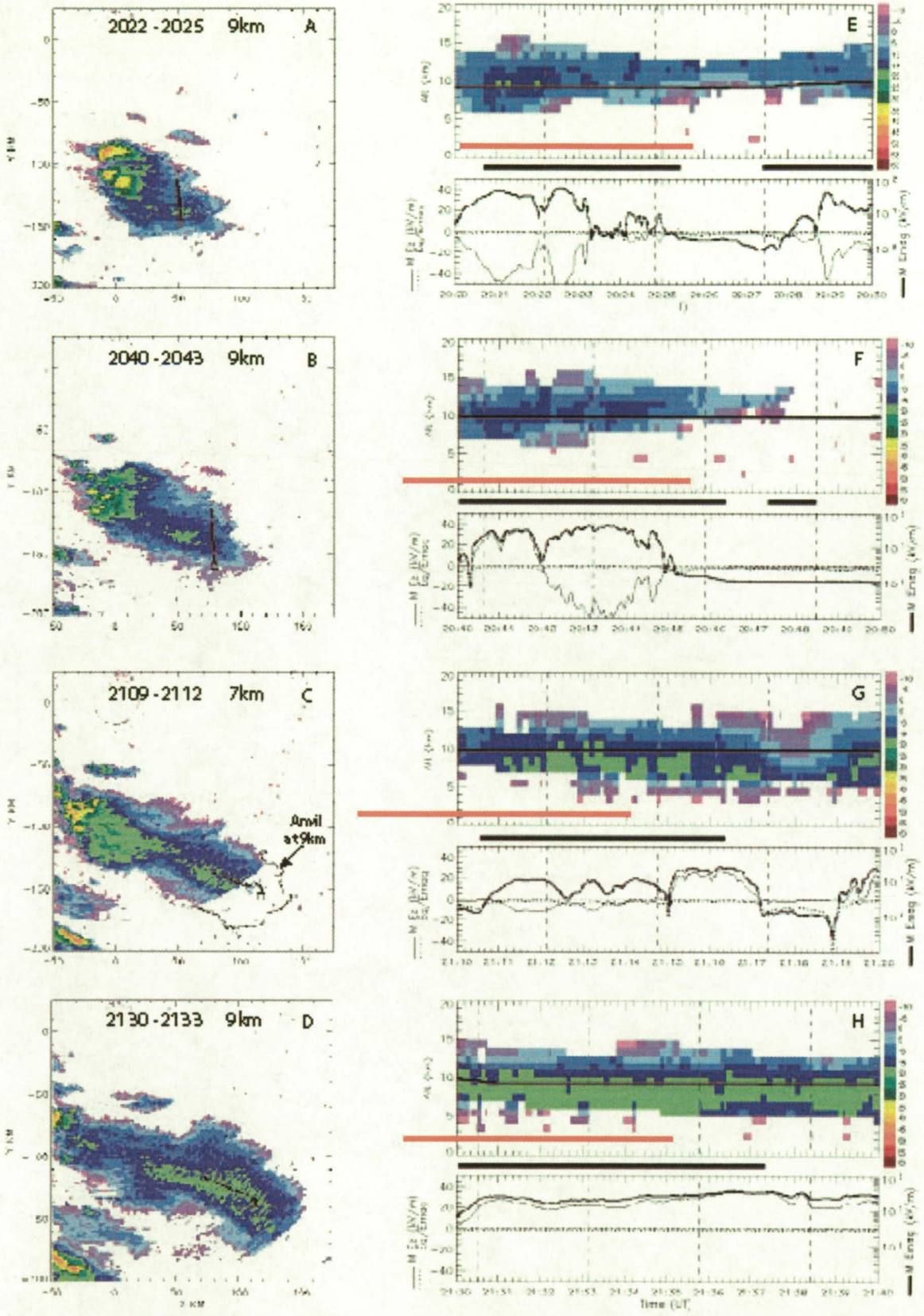

Fig. 5. As in Fig. 3, except CAPPIs from the WSR-74C radar for 4 June 2001 with 7 min

of aircraft track shown in black. The red bars below the reflectivity curtains in E, F, G and H correspond to the times of the aircraft track shown in A, B, C and D.

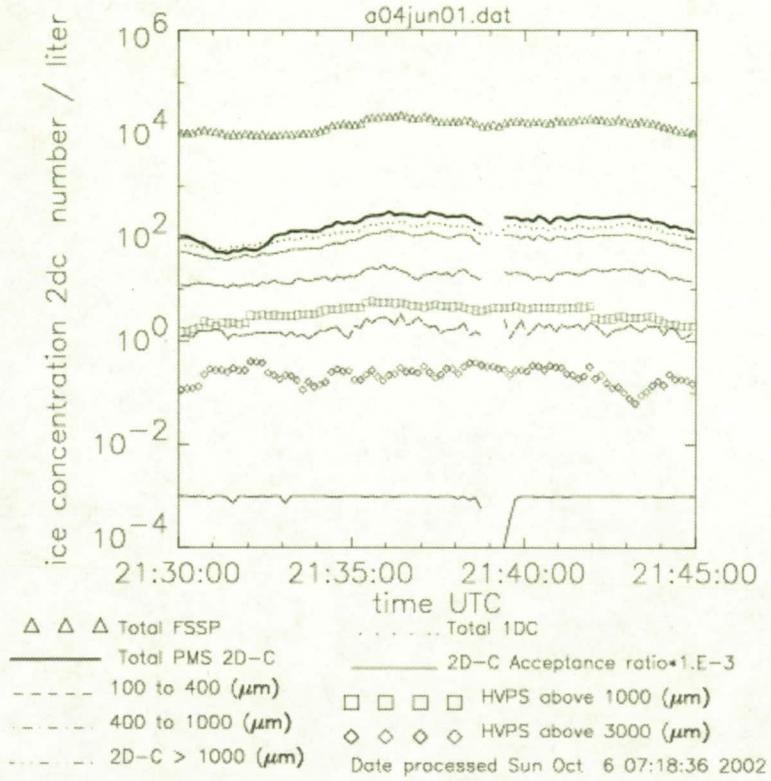

Fig. 6. Particle concentrations from different instruments in different size ranges as indicated for the period 2130 -2145, which includes the period corresponding to Figures 5D and 5H. The 2D-C malfunctioned near 2139.

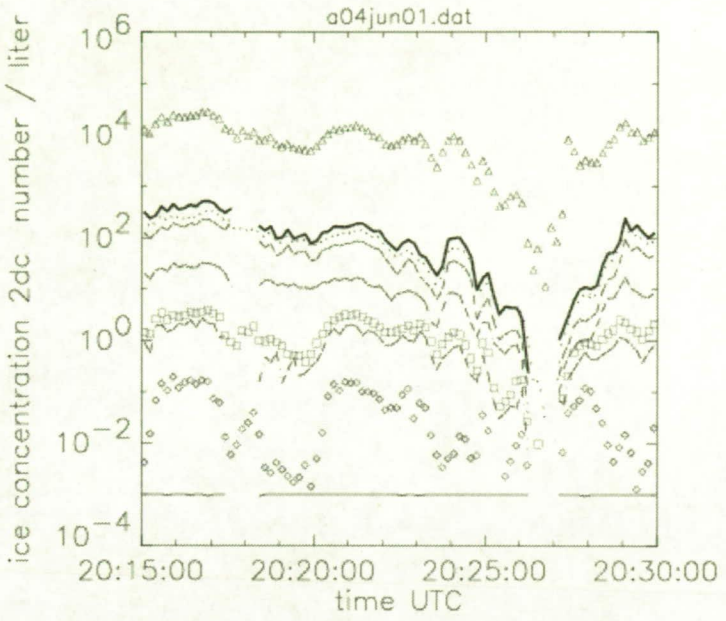

Fig. 7. As in figure 6, but showing measurements from 2015 to 2030 including the cross-anvil penetration from 2019 to 2026of figure 5A and 5H. The 2D-C malfunctioned near 2018.

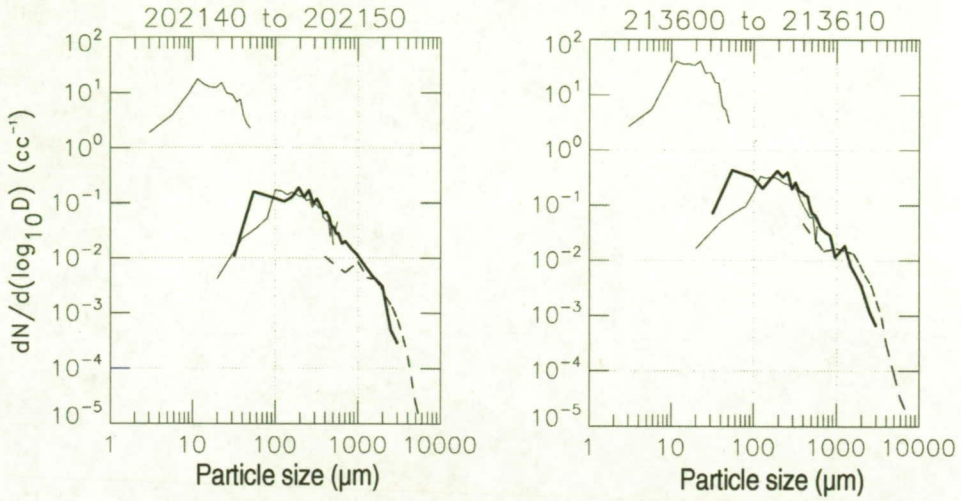

Figure 8. Particle size distributions measured on 4 June 2001 starting at 2021:40 (left) and 2136:00 (right). The light lines on the left of each plot are measurements from the FSSP. The bold line shows measurements from the 2D-Cloud probe, while the lighter line covering the same approximate size range are from the 1D-Cloud probe. The dashed curves on the right of each plot are from the High Volume Particle Sampler. See Dye et al. 2007 for further information on these probes and the ABFM II measurements.

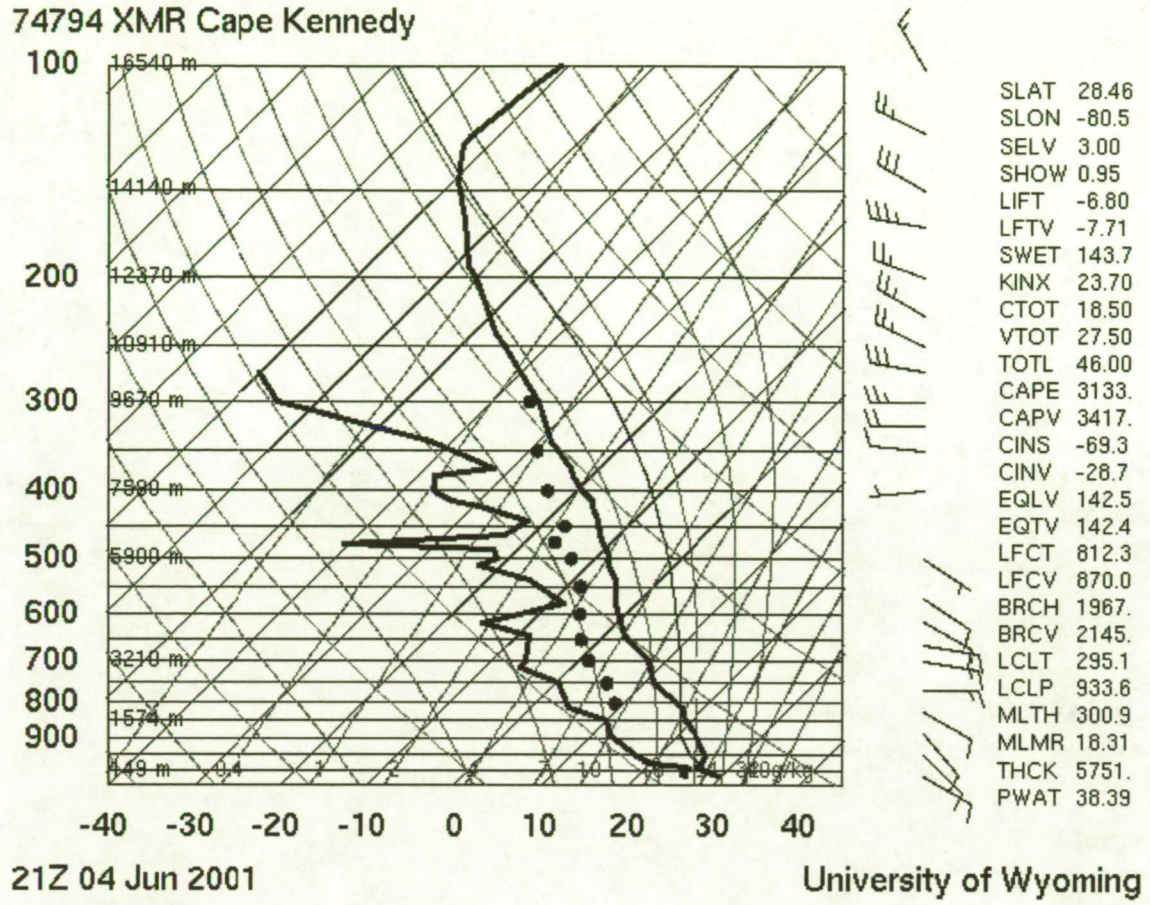

Figure 9. Environmental sounding from Cape Canaveral at 2100 on 4 June 2001. The temperature sounding is on the right with the dew-point temperature on the far left. The big dots between dew-point and temperature are graphically determined wet-bulb temperatures. Pressure (hPa) is on a logarithmic scale with labels to the far left. The corresponding altitude is labeled just to the right of the pressure. Temperature (^{o}C) is plotted as a skewed, solid line and labeled on the absicca.